JOURNAL OF PROPULSION AND POWER
Vol. 18, No. 4, July–August 2002

Mass Deposition Measurements from 26-Kilowatt Electric Propulsion Space Experiment Flight

G. G. Spanjers*
U.S. Air Force Research Laboratory, Edwards Air Force Base, California 93524-7013
J. H. Schilling†
Sparta, Inc., Edwards Air Force Base, California 93524-7013
S. F. Engelman‡
ERC, Inc., Edwards Air Force Base, California 93524-7013
D. R. Bromaghim§
U.S. Air Force Research Laboratory, Edwards Air Force Base, California 93524-7013
and
L. K. Johnson¶
The Aerospace Corporation, El Segundo, California 90245

The Electric Propulsion Space Experiment (ESEX) was launched and operated in early 1999 to demonstrate the compatibility and readiness of a 30-kW class ammonia arcjet for satellite propulsion applications. As part of the onboard sensor array, thermoelectric quartz crystal microbalances were used to measure material deposition at selected locations on the spacecraft surface. The sensors were held at a temperature that would allow them to condense metallic materials eroded from the electrodes, but that are insensitive to possible deposition of the propellant gas. The ESEX arcjet was fired eight times, constituting 33 min and 26 s of operating time. No material deposition was observed that could be attributed to nominal the arcjet firings, although during the first firing, significant deposition was observed near the arcjet nozzle. This deposition is attributed to contaminants within the arcjet body, collected during handling and storage, which were ejected during the first firing. For future programs, although engineering measures may be needed to protect spacecraft equipment in the immediate vicinity of the thruster body, the arcjet environment causes negligible deposition of electrode material.

I. Introduction

SPACECRAFT operation can be critically impaired by material deposition on vital surfaces. Deposition on thermal control surfaces can degrade emissive and absorptive properties and change the thermal balance of the satellite. Material deposition on solar cell cover glass can decrease transmissivity and degrade power generation capability. Understanding the coupling of these effects with high-power electric propulsion is of critical importance to the development of the next-generation of large U.S. Air Force (USAF) space structures. A major goal of the USAF Electric Propulsion Space Experiment (ESEX)[1] is to explore these issues by measuring the contamination effects of a 30-kW class arcjet in flight. ESEX was launched on 23 February 1999 as one of nine experiments aboard the Advanced Research and Global Observation Satellite.[2]

An array of sensors is positioned at strategic locations of the ESEX package to assess the contamination effects. Mass deposition is measured using four thermoelectric quartz crystal microbalances (TQCMs). Thermal flux from the arcjet firing is measured using four radiometers.[3] A sample gallium–arsenide (GaAs) solar array segment placed near the arcjet nozzle determines the impact on the satellite power generation capability.[4] Electromagnetic interference (EMI) is characterized using a set of onboard antennas and ground stations.[5] This paper focuses on mass deposition measurements from the TQCMs. Measurements from the other onboard sensors can be found in companion papers[3–5] within this issue.

During eight firings of the ESEX arcjet, no measurable material deposition is observed that is attributable to the steady-state operation of the arcjet. During arcjet firings, the mass deposited on each TQCM was observed to decrease slightly, suggesting that radiant heat from the arcjet was helping to vaporize previously deposited material. An exception occurred during the first firing, where significant deposition was observed near the arcjet nozzle. This anomalous deposition is attributed to contaminants within the arcjet body, collected during handling and storage, which were ejected during the first firing.

These ESEX mass deposition results are very promising for the integration of high-power electric propulsion on commercial and government satellites. The deposition effect observed is only on a sensor placed very near, and with a direct view of, the exhaust nozzle of the thruster and only on the first firing. It is highly unlikely that material or sensors would be located this close to the thruster's exit plane in an operational high-power, electric propulsion system. Deposition sensors located in the backplane of the arcjet show no deleterious effects. For future programs, although engineering measures may be needed to protect spacecraft equipment in the immediate vicinity of the thruster body, the arcjet environment is generally benign.

II. Mass Deposition Sensors

The ESEX flight unit is equipped with four TQCMs, four radiometers, and two sections of GaAs solar array cells. The sensors

Received 22 January 2001; revision received 2 January 2002; accepted for publication 27 January 2002.

*Project Scientist, Propulsion Directorate, AFRL/PRSS, 1 Ara Road. Member AIAA.
†Project Engineer, 1 Ara Road; currently Chief Scientist, W. E. Research, 4360 San Juan Court, Rosamond CA, 93560. Member AIAA.
‡Project Engineer, 1 Ara Road. Member AIAA.
§Electric Propulsion Space Experiment Program Manager, Propulsion Directorate, AFRL/PRSS, 1 Ara Road. Member AIAA.
¶Electric Propulsion Space Experiment Chief Scientist, 2350 E. El Segundo Boulevard; currently Research Scientist, Jet Propulsion Laboratory, Mail Stop 125-109, 4800 Oak Grove Drive, California Institute of Technology, Pasadena, CA 91109.

are positioned on the ESEX flight unit as shown in Fig. 1. Specific TQCM sensor locations are listed in Table 1. In Table 1, an angle equal to 0 is defined as horizontal to the thruster exit plane with negative values in the backflow region, and sensor angle is equal to 90 if the sensor normal is directed toward the thruster exit.

As shown in Fig. 1 and Ref. 4, TQCM 1 is positioned on the witness tower, adjacent to radiometer 1 and near the height of the thruster exit plane. TQCM 2 is located on the diagnostic deck below the thermal shield. TQCM 3 is located near the edge of the diagnostic deck and has a view of the arcjet plume. TQCM 4 is mounted on the deployable boom that also contains the EMI antenna. At the beginning of the flight, the boom was stowed and TQCM 4 faced the spacecraft surface. On Julian day 68.6, the boom was deployed. TQCM 4 then faced into the velocity vector (ram direction) of the spacecraft. Boom deployment was verified by a response from the onboard accelerometer[1] and by a subsequent decrease in the collected mass on TQCM 4 indicative of the atomic oxygen erosion expected for a ram-facing surface.

Each TQCM package includes a sensor crystal, reference crystal, and electronics. The sensor crystal is a piezoelectric quartz crystal, driven by an electronic oscillator attached to two metal plates placed on both sides of the quartz blank. The oscillator imposes a time-dependant electric field between the plates, which drives an acoustic oscillation in the crystal at a frequency determined by the total thickness of the crystal plus any mass on the outsides of these electrodes. The frequency of the crystal decreases as mass is added, providing a highly sensitive measurement of mass collection on the sensor face. The reference crystal is positioned immediately behind the sensor crystal and shielded from interaction with the space environment. Electronics within the TQCM drive the oscillations and measure the resonant frequencies of each of the crystals. The two

Table 1 Locations of TQCM sensors relative to arcjet exhaust plane

TQCM no.	Distance, cm	Angle, deg	Sensor angle, deg	Comment
1	40	−11	79	
2	45	−60	60	Under radiation shield
3	59	−40	40	
4	93	−19	19	On deployable boom

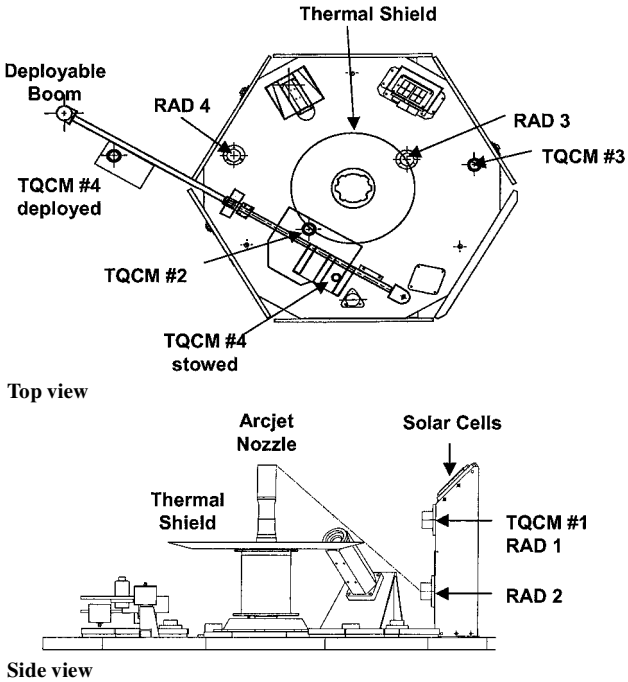

Fig. 1 ESEX showing the locations of the contamination sensors; arcjet exhaust is directed toward the top of the page.

crystal frequencies are electronically mixed and filtered to output the beat frequency, equal to the difference between the two frequencies. As mass is accumulated on the sensor crystal, the resonant frequency decreases and the beat frequency between the two crystals increases. Thus, an observed increase in the output frequency of the TQCM is associated with an increase in mass at the sensor crystal.

The sensor crystal is approximately 0.0168 cm thick, with an active area of 0.317 cm^2, and is gold plated. The sensor has a signal response of 4.49×10^{-9} $g/cm^2 \cdot Hz$. For a hypothetical contaminant density of 1 g/cm^3, this corresponds to a deposition thickness of 0.44 Å/Hz. The absolute sensor measurement uncertainty is 0.2 Hz (Ref. 6).

The four ESEX TQCMs are the MK-10 Model from QCM Research and were chosen to be identical to those used on the Midcourse Space Experiment (MSX) Satellite[7] launched in 1996. The only difference between the TQCMs on MSX and those on ESEX is that the MSX sensors used a 15-MHz crystal, whereas the ESEX sensors use the 10-MHz crystals. The ESEX program could, thus, take advantage of the characterization and calibration work performed by the MSX team before flight.[8] The critical characterization was to determine the long-term drift rate of the sensors, which can be influenced by crystal aging, changes in the performance of the electronics, and the oscillator thermal design. During a 21-day drift test, the MSX characterization showed a cyclic 4-Hz variation in the sensor output frequency.

For the ESEX data, the 4-Hz uncertainty due to drift is appropriate for long-term measurements of contaminants due to effects such as spacecraft outgassing. The lower 0.2-Hz uncertainty is appropriate for short-duration events such as the sensor response to a short (~15 min) arcjet firing. The frequency response of the TQCM is on the order of microseconds and not an issue for the ESEX measurements.

Exposure of the TQCM sensor crystal to radiation from the sun or the arcjet firing affects the oscillation frequency by creating a temperature gradient across the crystal diameter.[6,8] Each time the sun comes into the field of view, the sensor crystal will reflect some of the radiation, but also partly absorb the radiation, causing a thermal gradient and, thus, a frequency change. The effect is temporary, with the sensor crystal returning to the original frequency when the radiation source is removed. From an operations perspective, this insolation effect causes the output beat frequency to oscillate with the frequency of the orbital cycle and with amplitude dependent on the solar flux at each sensor. An example is shown in Fig. 2, where the beat frequency for TQCM 1 is plotted over two days. The solar flux causes an oscillation amplitude of about 200 Hz whereas mass change on the sensor face causes the slow 30-Hz rise observed over the two days. The amplitude of the beat frequency oscillation due to cyclic solar flux for TQCM sensors 2, 3, and 4 is approximately 160, 130, and 160 Hz, respectively. The frequency change due to mass deposition can be deconvoluted from the insolation oscillations by either subtracting the solar oscillation effects, or by using data from the same relative time during each orbit. For the present analysis, we use either the latter technique, or simply show the full oscillation.

The TQCMs can be controlled to temperatures between 193 and 353 K, strongly dependent on the heat sink temperatures. Preflight ESEX thermal analysis indicated that temperatures as low as 173 K might be achieved on-orbit for sensors 2 and 3. During the ESEX flight, a minimum temperature of 193 K was achieved on all four sensors, but it could not be maintained through the solar cycle. A 210-K temperature was found to be maintainable through the solar cycle. To reduce the potential for temperature oscillations during an arcjet firing, where the TQCM heat sink is subjected to additional thermal flux, the TQCM sensor temperature was adjusted to 218 K and maintained through the ESEX experiment. The TQCM sensors are baked off by increasing the temperature to vaporize some of the condensed material. When the temperatures at which the deposited mass is reduced to vapor pressure curves of the candidate specie are compared, the composition of the deposited material may, in principle, be determined. A total of seven bake-offs at temperatures of

298 and 322 K were performed between Julian days 54 and 120. In general, it was found that very little mass could be removed through the bakeoff process. Further, details of the frequency change during bakeoff were convoluted by the sensor insolation during the solar cycle. This prevented the conclusive identification of individual species that may have been vaporized during the bakeoff process.

Mass deposition (or loss) measured by the TQCMs can be a result of several physical processes including condensation, vaporization, absorption, chemical reaction into more/less volatile molecules, energy deposition releasing previously collected material, sputtering, etc. In this analysis we refer to a change in the TQCM sensor mass as a generic mass deposition without attempting to identify a specific physical process for the observed mass increase or loss. We also distinguish between a TQCM frequency change and mass deposition. For example, the frequency change due to the insolation effect is clearly not indicative of a mass change of the sensor crystal. Graphs of data used to illustrate frequency changes that are not necessarily due to a mass change are plotted in terms of the beat frequency output from the TQCM, for example, Figs. 2–4 and 7. Graphs that ignore the insolation effect by illustrating the trend of the oscillation amplitude are plotted in terms of mass deposition, for example, Figs. 5 and 6. All temporal plots are in terms of Julian days, where the calendar days are numbered sequentially, starting with day 1 on 1 January and continuing through to day 365 on 31 December for a nonleap year.

III. Flight Data

The ARGOS host spacecraft for ESEX was launched 23 February 1999 from Vandenberg Air Force Base using a Delta II launcher into a 97-deg, near-polar orbit at 846-km altitude. The ESEX contamination diagnostics were turned on to collect data 1 h, 25 min after launch. The TQCMs were first commanded to cool 8 h, 14 min after launch, to enable measurements of the spacecraft outgassing during the vehicle initialization and check out. A total of eight ESEX firings were performed between 15 March 1999 and 21 April 1999. Following the eighth firing, a battery anomaly occurred, which precluded additional firings. The ESEX events, including the battery anomaly, are described in detail in a companion paper in this issue.[1]

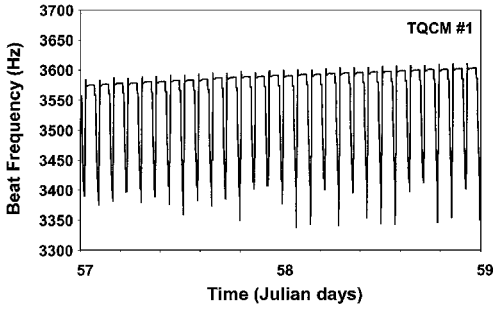

Fig. 2 Representative TQCM data showing the slow frequency increase due to mass deposition superimposed on the larger solar cycle oscillations.

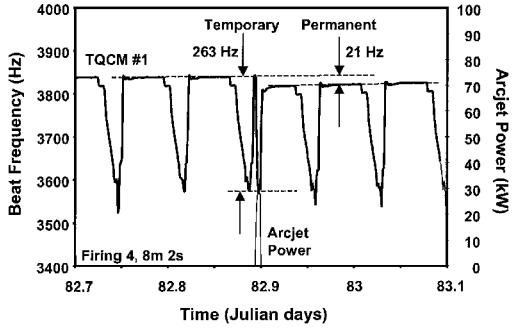

Fig. 3 Typical TQCM response to an arcjet firing: output frequency from TQCM 1 during firing 4.

Table 2 Contamination events during ESEX flight experiment

Firing (F) or event	Date/Time (zulu)	Julian date	Duration
Boom deployed	9 March 1999 14:59:57	68.62497	
F-1C	15 March 1999 21:55:55	74.91383	2 m, 21 s
F-2	19 March 1999 22:32:23	78.93916	5 m, 1 s
F-3	21 March 1999 12:24:41	80.51714	5 m, 33 s
F-4	23 March 1999 21:27:57	82.89441	8 m, 2 s
F-5	26 March 1999 12:45:25	85.53154	6 m, 4 s
F-6	31 March 1999 13:05:37	90.54557	4 m, 29 s
F-7	02 April 1999 22:09:03	92.92295	53 s 38 s
F-8	21 April 1999 12:22:12	111.51542	42 s
Battery anomaly	22 April 1999 15:18:37	112.63793	

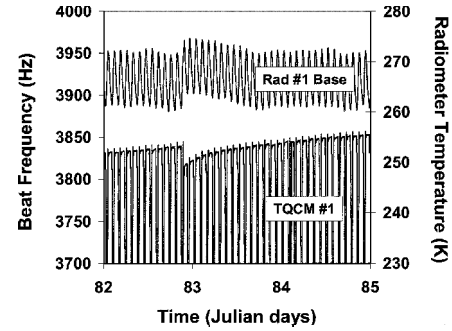

Fig. 4 TQCM 1 response to firing 4 shown with a longer time base and local spacecraft temperature measured at the base of adjacent radiometer 1.

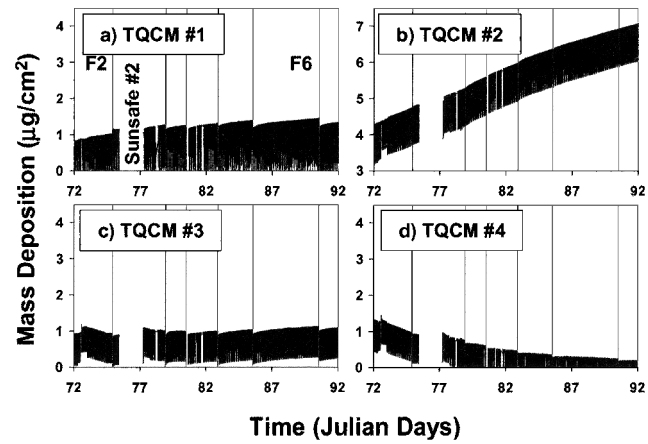

Fig. 5 Mass deposition measured on each of the four TQCMs through the six primary ESEX firings.

A summary of the ESEX events related to the contamination measurements is shown in Table 2.

In general, the TQCM data show three effects in response to arcjet firings. Two of these are apparent in Fig. 3, which shows an expanded view of the TQCM response to firing 4. A sharp frequency decrease of 263 Hz (mass equivalent of 1.18 μg/cm^2) is observed coincident with the arcjet power. For identification purposes, this will be referred to as the temporary frequency change. Following the firing, a smaller permanent frequency decrease of 21 Hz (mass equivalent of 94.9 ng/cm^2) is apparent. The third effect is shown in the same plot for TQCM 1, shown on a slightly longer timescale

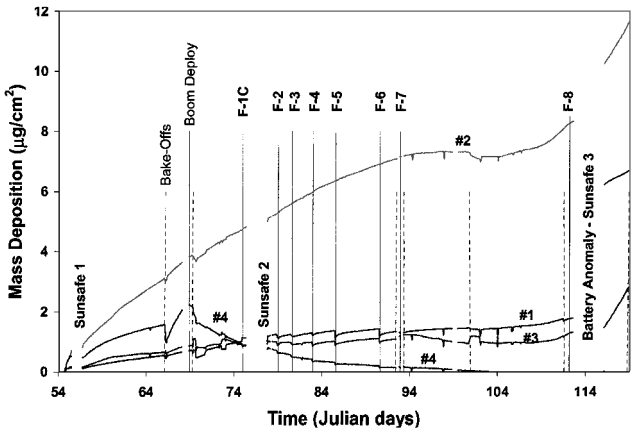

Fig. 6 TQCM behavior from launch through the battery anomaly.

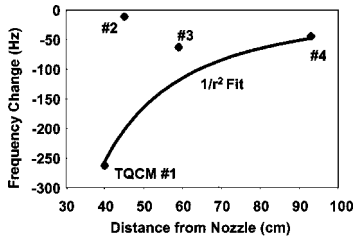

a) Temporary frequency change

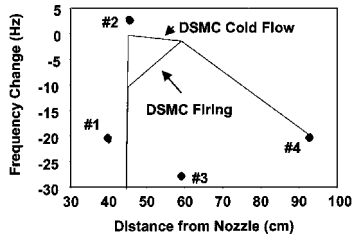

b) Permanent frequency change

Fig. 7 TQCM frequency changes during arcjet firings.

in Fig. 4. Following the firing, the TQCM experiences a period of increased mass deposition rate, evidenced by the increased slope in the sensor frequency vs time. This increased deposition rate lasts for about one day and is accompanied by an increase in the surrounding temperature, as measured at the base of the adjacent radiometer 1 and coplotted with the TQCM 1 frequency.

Figure 5 shows the response of each of the four TQCMs to the six arcjet firings with duration greater than 2 min. In general, behavior similar to that described earlier is seen for each firing (F) with two exceptions. TQCM 1, located on the witness tower and viewing the arcjet nozzle, shows a 140-ng/cm^2 jump in mass deposition with the first firing (F-1C, 141 s). Because similar jumps are not apparent on the subsequent firings (F-2–6), this jump is attributed uniquely to the first firing of the arcjet and not an indicator of steady-state operation. TQCM 2, shielded by the arcjet thermal shield, shows no permanent frequency decrease from the firings, but does exhibit the one-day period of increased deposition following each firing. The temporary frequency decreases coincident with the arcjet firings are not visible on the longer time base shown in Fig. 5.

The TQCM mass deposition recorded from shortly after launch through the battery anomaly is shown in Fig. 6. Each of the TQCMs shows a rapid rise shortly after launch that decays in time, indicative of a decreasing outgassing rate from the spacecraft. Bakeoff events, denoted by the vertical dashed lines, correspond to times when the TQCM sensors are commanded to heat in an attempt to vaporize off collected mass. Sunsafe modes of the satellite are accompanied by a data dropout and typically a decrease in the total mass deposition. The mass decrease is attributable to the TQCM temperature rising due to the loss of power during the sunsafe event, resulting in material bakeoff. TQCM 4 starts the flight with a mass deposition rate that is likely the best indicator of the spacecraft cleanliness because the sensor is directed toward the spacecraft surface before boom deployment. After boom deployment, when the sensor faces the spacecraft ram direction, the mass deposition decreases, presumably a result of atomic oxygen erosion.

Not surprisingly, the TQCMs show a strong response to the battery anomaly. TQCM 3 exhibits a strong increase in deposition rate. TQCM 1 shows a discreet jump in mass collected through the event. TQCM 2 also shows a dramatic increase in both mass deposition and the deposition rate. It is interesting that TQCM 2 exhibits a higher deposition rate several days in advance of the anomaly and, in retrospect, may have been a precursor to the event.

IV. Discussion

With each firing (except F-1 on TQCM 1), TQCMs 1, 3, and 4 show a pronounced decrease in mass deposition, whereas obscured sensor TQCM 2 shows no effect. Following the firing, each sensor exhibits a period of increased mass deposition rate. When possible sources for the frequency changes and the expected magnitude of the changes at each sensor are examined, the cause of various TQCM effects can be postulated. Candidate influences that can affect the sensor frequency (other than mass deposition) are a local temperature rise, radiative impingement from the plume, atomic oxygen erosion, and the expulsion of reactive species that act to remove deposited mass.

The influence of a local temperature rise acts to increase the mass deposition rate by increasing the local outgassing rate. A similar effect is observed when the TQCM temperature is changed. When the TQCM sensor is cooled, heat rejection heats the surrounding area, and a period of increased mass deposition rate is observed until thermal equilibrium is reached. Following each firing, ESEX temperatures are elevated for about one day. This effect is believed to be the source of the increased mass deposition rate following the firing shown in Fig. 4. The elevated ESEX temperatures are apparent in the radiometer 1 base temperature also shown in Fig. 4.

For radiative impingement, one would expect the effect to scale with distance squared from the thruster exit. Figure 7a shows the temporary frequency change vs distance from the arcjet nozzle, associated with F-4 for each TQCM. Also shown is a $1/r^2$ curve expected for frequency changes attributable to radiative impingement from the arcjet. The curve is forced to go through the data point for TQCM 1. The $1/r^2$ fit agrees with the data for TQCM 4. TQCM 2 is well below the curve in magnitude, as expected, because the thermal shield blocks the sensor's view of the arcjet body and plume. TQCM 3 is slightly below the curve; however, this might be expected because the thermal shield blocks the TQCM 3 view of the arcjet body, thus decreasing the radiative intensity at the sensor. Based on these data, the temporary frequency change that is observed during each firing is believed to be a result of radiative impingement from the arcjet plume and body.

The permanent frequency change observed during F-4 is shown in Fig. 7b. Clearly a radiative model will not fit these data because TQCMs 3 and 4 show effects similar in magnitude to TQCM 1. Thermal effects will not fit because TQCM 2 experiences a local temperature increase about equal to the other sensors, but shows minimal frequency change. For interaction with an expelled reactive specie, one would expect the frequency change to be proportional to the local density, which can be estimated through direct simulation Monte Carlo (DSMC) simulations. Shown in Fig. 7b are predictions from a cold-flow DSMC analysis[9] and a DSMC analysis that includes the effects of the arcjet firing.[10] Both DSMC plots are forced through the data point for TQCM 4. The DSMC analysis shows the decreased response for TQCM 2 relative to TQCMs 1 and 4 in agreement with the data. Contrary to the models, TQCM 1 shows a response about 10 times below that predicted by DSMC analysis. Clearly, none of the three influences can be used alone to explain the permanent frequency change observed after each firing. It is presumed that a combination of thermal, radiative impingement, reactive species, atomic oxygen, and other effects acting in concert to achieve the frequency changes observed experimentally.

V. Summary

Analysis of the data from the ESEX flight is performed to assess mass deposition associated with the use of the 30-kW arcjet. No material deposition is observed for surfaces held at 218 K, with the exception of a sensor very near the arcjet nozzle, which showed deposition only for the first firing. The thermal heat load from firing the 30-kW thruster does lead to an elevated spacecraft temperature, which increases the outgassing rate and, hence, the mass deposition on the sensors. The latter effect can be tempered through improved thermal design to block radiative impingement to the spacecraft surfaces.

In general, a mass deposition effect was observed only for a sensor placed very near the arcjet nozzle, much closer than would be designed on an operational spacecraft. Sensors placed in the thruster backplane showed no mass deposition effects associated with the arcjet firing. The ESEX data suggest that the mass deposition contamination associated with the operation of high-power electric propulsion can be controlled through relatively simple design adjustments.

Acknowledgments

The authors would like to extend their gratitude for the expert technical contributions of Mary Kriebel, Don Baxter, Bob Tobias, David Lee, David Huang, and N. John Stevens of TRW in the design and development of the flight diagnostic package. Dave White of W.E. Research provided excellent technical support collecting the Electric Propulsion Space Experiment data from the Advanced Research and Global Observation Satellite (ARGOS) spacecraft telemetry. We also acknowledge the ARGOS program office and the flight operations team at Kirtland Air Force Base for their technical expertise, as well as their insight and flexibility in the mission operations. Scott Wallace of QCM Research also provided technical assistance on the use of the thermoelectrically cooled quartz crystal microbalances. Iain Boyd of the University of Michigan provided assistance in the application of plume models.

References

[1]Bromaghim, D. R., Le Duc, J. R., Salasovich, R. M., Spanjers, G. G., Fife, J. M., Dulligan, M. J., Schilling, J. H., White, D. C., and Johnson, L. K., "Review of the Electric Propulsion Space Experiment Program," *Journal of Propulsion and Power*, 2002; also AIAA Paper 99-2706, June 1999.

[2]Turner, B. J., and Agardy, F. J., "Advanced Research and Global Observation Satellite (ARGOS) Program," AIAA Paper 94-4580, Sept. 1994.

[3]Spanjers, G. G., Schilling, J. H., Bromaghim, D. B., and Johnson, L. K., "Radiometric Analysis from the 26-Kilowatt Electric Propulsion Space Experiment Flight," *Journal of Propulsion and Power*, 2002.

[4]Schilling, J. H., Spanjers, G. G., Bromaghim, D. B., and Johnson, L. K., "Solar Cell Degradation During the 26-Kilowatt Electric Propulsion Space Experiment Flight," *Journal of Propulsion and Power*, 2002.

[5]Dulligan, M. J., Bromaghim, D. B., Zimmerman, J. A., Salasovich, R. M., Hardesty, D., and Johnson, L. K., "Effect of Electric Propulsion Space Experiment 26-Kilowatt Arcjet Operations on Communications," *Journal of Propulsion*, 2002.

[6]Wallace, D. A., and Wallace, S. A., "QCM Research Operating Manual—Mark 10," QCM Research, Laguna Beach, CA, 1996.

[7]Wood, B. E., Hall, D. F., Lesho, J. C., Uy, O. M., Dyer, J. S., and Bertrand, W. T., "MSX Satellite Flight Measurements of Contamination Deposition on a CQCM and on TQCMs," AIAA Paper 97-0841, Jan. 1997.

[8]Bryson, R. J., Seiber, B. L., Bertrand, W. T., Jones, J. H., and Wood, B. E., "MSX Thermoelectric Quartz Crystal Microbalances—Calibration and Characterization," Society of Photo-Optical Instrumentation Engineers, SPIE Paper 2261-25, 1994.

[9]Boyd, I. D., Kannenberg, K. C., Kossi, K. K., Levin, D. A., and Weaver, D. P., "Modeling the Plume Contamination and Emissions of an Ammonia Arcjet," AIAA Paper 98-3505, 1998.

[10]Kriebel, M. M., and Stevens, N. J., "30-kW Class Arcjet Advanced Technology Transition Demonstration (ATTD) Flight Experiment Diagnostic Package," AIAA Paper 92-3561, July 1992.